CONF-880372--1

BRILLOUIN SCATTERING AT HIGH PRESSURES

M. Grimsditch

Materials Science Division

Argonne National Laboratory,* Argonne, Illinois 60439

and

A. Polian

Physique des Milieux Condenses

Universite P. et. M. Curie, 4 Place Jussieu T13 E4, 75230 Paris

February 1988

CONF-880372--1

DE88 011972

DISCLAIMER

Submitted to Proc. of the NATO Advanced Research Workshop on "Simple Molecular Systems at Very High Density", Les Houches, March 28-April 5, 1988.

*Work supported by the U.S. Department of Energy, BES-Materials Sciences, under Contract #W-31-109-ENG-38.

BRILLOUIN SCATTERING AT HIGH PRESSURES

M. Grimsditch* and A. Polian**

*Materials Science Division, Argonne National Laboratory, Argonne, IL 60439, **Physique des Milieux Condenses, Univ. P. et. M. Curie, 4 Place Jussieu T13 E4, 75230 Paris

ABSTRACT

Technical advances which have made Brillouin scattering a useful tool in high pressure diamond anvil cell (DAC) studies, viz. multipassing and tandem operation of Fabry-Perot interferometers, are reviewed. Experimental aspects, such as allowed scattering geometries, are outlined and the data analysis required to transform Brillouin spectra into sound velocities and elastic constants is presented.

Experimental results on H_2, N_2, Ar, and He are presented, and the close relationship between the Brillouin scattering results and equations of state is highlighted.

I. INTRODUCTION

Brillouin scattering is the inelastic interaction of light with thermal acoustic phonons in a material. This interaction, which involves the creation or annihilation of phonons, results in a shift in the frequency of the scattered radiation. Hence, by measuring the changes in frequency in the scattered radiation, information is obtained on the phonons in the material. Details of the physical mechanism involved in the scattering process, which yields cross-sections, selection rules etc., can be found in the literature.[1-3] Here it will suffice to consider only the simple relation that can be invoked just on the basis of conservation of energy and momentum. Let ω and $\vec{k}$ designate the frequency and wavevector of the radiation and let subscripts i and s indicate "incident" and "scattered" respectively. The frequency and wavevector of the phonons are Ω and $\vec{q}$. From energy conservation we have

$$\hbar\Omega = \pm \hbar (\omega_i - \omega_s) \qquad (1)$$

and from wavevector conservation

$$\vec{q} = \pm (\vec{k}_i - \vec{k}_s) \qquad (2)$$

where the + sign applies to the creation (Stokes) and the - sign to the annihilation (anti-Stokes) of a phonon. The fact that Eqs. 1 and 2 are the same as those used to describe Raman scattering should not be surprising since the physical phenomenon is the same in both cases. The distinction between them is entirely historical and is only because Brillouin[4] predicted the scattering of light by acoustic phonons in 1914 (not observed experimentally until 1930 by Gross[5]) and Raman[6] observed frequency shifted scattered light in 1928 (not identified as due to optical phonons until later).

From the experimental point of view however, there is a substantial difference between Brillouin and Raman scattering. In the former, where frequency changes are of the order of ~1 cm^{-1}, it is necessary to use a Fabry-Perot interferometer to obtain the necessary resolution. In the latter, typical frequency shifts of ~100 cm^{-1} can readily be resolved with a grating instrument.

In section II the advances in Fabry-Perot spectroscopy which have made it a powerful tool in solid state physics, are briefly reviewed. Section III covers some specific aspects of Brillouin scattering such as scattering geometries, and data analysis. Details dealing specifically with the application of Brillouin scattering to the investigation of materials at high pressures in DAC is covered in Sec. IV and in Sec. V experimental results on H_2, N_2, Ar, and He are reviewed.

II. FABRY-PEROT SPECTROSCOPY

As mentioned in the previous section, the most convenient instrument to use when a resolution better than 1 cm^{-1} is required is a Fabry-Perot (FP) interferometer. This instrument consists of two plane partially transmitting mirrors separated by a distance d. In the form in which it is most commonly used nowdays, a parallel beam of radiation which is to be frequency analyzed is incident along the mirror axes; since transmission occurs only when

$$2d = p\,\lambda \tag{3}$$

where λ is the wavelength of the radiation and p is an integer, by changing d the wavelength of the radiation being transmitted is selected. The transmitted intensity as a function of the change in distance d predicted by Eq. 3 is shown schematically in Fig. 1a. However Eq. 3 is derived assuming perfectly flat and reflecting mirrors and also that the incident beam is perfectly parallel, in reality, because these conditions are not strictly true, the transmission curves look like that shown in Fig. 1b.

Transmission curves like the one in Fig. 1b lead to the definition of some of the important parameters that describe a working instrument. These are: contrast (C) defined as the ratio of the maximum to minimum transmission, and finesse (F) defined as the ratio of the distance between peaks to the peak width. The contrast of an instrument is important because it determines the maximum intensity ratio between two spectral components that can be resolved. The finesse is related to the maximum number of spectral components that can be resolved simultaneously.

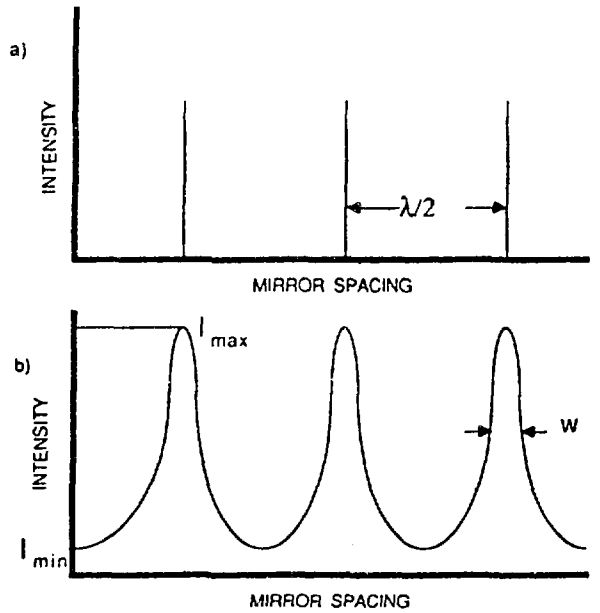

Fig. 1. Transmission function of a Fabry-Perot: The upper portion is for an idealized instrument, the lower portion is typical for a real instrument.

The conversion of the horizontal axis to a frequency scale is simple since it can be shown that the distance between too successive peaks corresponds to a frequency change of c/2d (c is the velocity of light). This quantity is called the free spectral range (FSR).

The most severe drawback in the use of a FP such as that described above to solid state problems is its contrast. Typically only contrasts of a few hundreds can be obtained and this is only sufficient to observe the Brillouin lines in transparent materials of exceptionally high quality. It is worthwhile noting that in a perfect crystal there should be no scattered light at the incident frequency and that the observed unshifted radiation (usually many many orders of magnitude stronger than the Brillouin components) is produced entirely by the presence of defects, cracks, surfaces, etc.

The conceptually simple solution of placing two instruments in series (thereby squaring the contrast), a well known technique in Raman scattering where double- and triple-monochromators are common, poses such severe constraints on synchronization that no adequate solution was found until 1971 when Sandercock[7,8] showed that the same instrument could be used for successive passes thus avoiding all problems of synchronization! Not only could the instrument be double-passed in this fashion but up to seven passes were performed yielding contrasts in excess of 10^{10}. This single

improvement changed Fabry-Perot interferometry from an almost academic curiosity in the field of solid state physics to a powerful tool for the investigation of condensed matter.

Another considerable disadvantage of FP interferometry is the fact that its transmission function is multivalued. This means that from a single measurement the frequency difference between two lines can only be determined modulo one FSR. Conversely, two spectral features which differ in frequency by an integral number of FSR's will overlap in the spectrum. When a large number of spectral features are present, this overlapping can lead to considerable difficulty in interpreting the spectra. A solution to this problem was also produced by Sandercock[8] who implemented a practical technique for synchronously scanning two Fabry-Perot's. Without going into detail, the result of scanning two interferometers with <u>different</u> spacings essentially eliminates the problem of overlap between different orders. Spectra exhibiting the crucial nature of this technical achievement will be shown in a later section.

III. BASICS OF BRILLOUIN SCATTERING

As mentioned briefly in the Introduction, Brillouin scattering provides information on the acoustic branches of the phonon dispersion curves. In this respect, it provides the same information obtained in ultrasonic experiments. From Eq. 1 we know that the frequency shift of the scattered radiation is equal to that of the phonon being probed. Using Eq. 2 the wavevector of the phonon can be determined; thus immediately yielding the sound velocity (v)

Table I. Effective elastic constant (X), polarization ($\vec{u}$) and scattering tensor (T) for phonons propagating along a [110] direction of a cubic crystal.

X	$\vec{u}$	T
$(C_{11} + C_{12} + 2C_{44})/2$	[110] long. (L)	$\begin{vmatrix} p_{11}+p_{12} & 2p_{44} & 0 \\ 2p_{44} & p_{11}+p_{12} & 0 \\ 0 & 0 & 2p_{12} \end{vmatrix}$
C_{44}	[001] transv. (T_1)	$\begin{vmatrix} 0 & 0 & p_{44} \\ 0 & 0 & p_{44} \\ p_{44} & p_{44} & 0 \end{vmatrix}$ $\sqrt{2}$
$(C_{11} - C_{12})/2$	[1$\bar{1}$0] transv. (T_2)	$\begin{vmatrix} p_{11}-p_{12} & 0 & 0 \\ 0 & -(p_{11}-p_{12}) & 0 \\ 0 & 0 & 0 \end{vmatrix}$

$$v = \Omega/q \ . \qquad (4)$$

The sound velocity in turn allows the determination of the elastic constants which relate stresses and strains in a given material. For a given sound wave the solution of the equations of motion show that

$$X = v^2\rho \qquad (5)$$

where X is an effective elastic constant and ρ is the density. For the sake of an example: if an experiment is performed so that phonons propagating along a [110] direction in a cubic crystal are probed, the corresponding values of X in terms of the components of the elastic constant tensor (C_{ij}) are given in Table I. Hence, like in any ultrasonic experiment, by measuring an appropriate set of directions all the components C_{ij} can be determined. It is worthwhile noting that since the accuracy of ultrasonic experiments is orders of magnitude better than that of Brillouin scattering, the latter should only be considered if the use of ultrasonic techniques is not possible e.g., experiments in diamond anvil cells.

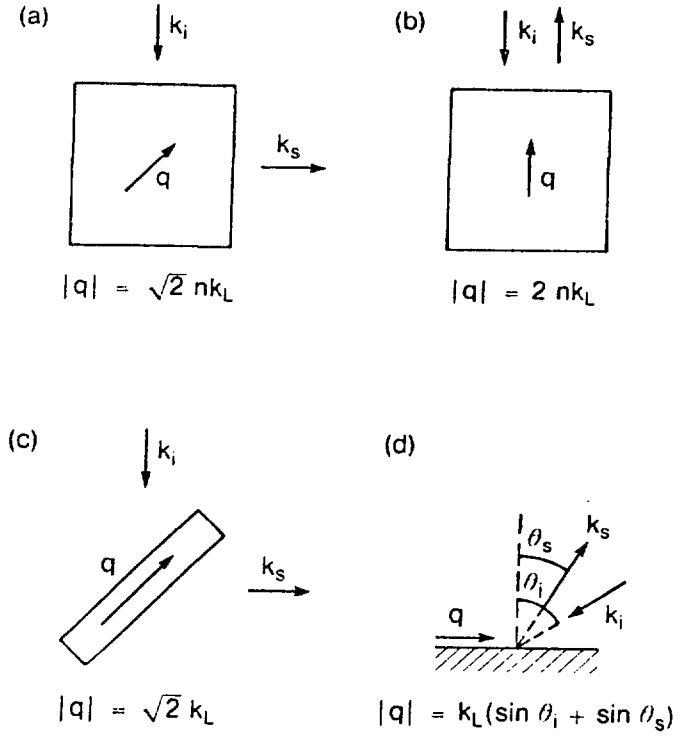

Fig. 2. Most commonly used scattering geometries in Brillouin scattering: a) 90° scattering; b) backscattering; c) platelet geometry; and d) surface wave geometry (this last geometry is used for opaque materials). k indicates the wavevector of the incident and scattered light, q that of the phonon.

Figure 2 shows a number of scattering geometries which are often utilized in Brillouin scattering experiments. The vectors k_i and k_s represent the wavevectors of the incident and scattered light, n is the refractive index and q is the phonon wavevector with its direction and magnitude calculated from Eq. 2 also indicated (the values given for $|q|$ assume optical isotropy of the material under study, more general expressions exist for cases of lower symmetry). Figures 2a-2c are used in cases of transparent samples, Fig. 2d for opaque materials: the latter case will not be considered further in this article. From Fig. 2 it is clear that if the crystallographic orientation of the sample is known relative to $\vec{k}_i$ and $\vec{k}_s$ the phonon propagation direction $\vec{q}$ is also known. Once $\vec{q}$ is known the characteristics of the phonons propagating along that direction can be calculated.[9] In general three solutions will be found corresponding to the three possible orthogonal polarizations of the phonon. As an example Table I summarizes the results for propagation along a [110] direction in a cubic crystal. The sound velocity (v) is related to X through Eq. 5 and the phonon polarization, denoted by $\vec{u}$, indicates the direction of motion of the atoms associated with the phonon.

Once the polarization of a phonon is known, its amplitude (A) can be written as

$$A = A_o \vec{u}\, e^{i(\vec{q}\cdot\vec{r} - \Omega t)} \tag{6}$$

From this expression the elastic strains produced by the phonon can be calculated. Since the changes in dielectric constant ($\varepsilon_{\ell m}$) are related to the strains (η_{ij}) through

$$\Delta\varepsilon_{\ell m} \propto p_{\ell m i j}\, \eta_{ij} , \tag{7}$$

the change (T) in the dielectric constant tensor produced by each phonon can be calculated. These are given for phonons with $\vec{q}$ along [110] in Table I. Values of X, $\vec{u}$ and T for other propagation directions and crystal symmetries can be found in Ref. 3.

The scattered intensity (I) is related to the tensor T through

$$I \propto [e_i \cdot T \cdot e_s]^2 \tag{8}$$

where e_i and e_s are the polarizations of the incident and scattered light.

For the sake of an example we consider the following two cases: (i) Backscattering along a [110] direction (i.e., $\vec{k}_i = -\vec{k}_s // [110]$). This corresponds to the geometry of Fig. 2b and probes phonons propagating along [110] so that we can use the tensors given in Table I. The possible polarization of the incident and scattered light are [001] and [1$\bar{1}$0]; using Eq. 8 the expected intensities are given in the upper portion of Table II. (ii) 90° scattering with $k_i // [001]$ and $k_s // [010]$ corresponding to the geometry of Fig. 2a which also probes phonons along [110]. The possible polarizations of the incident light are [010] and [001] those of the scattered light [100] and [001]. The expected intensities for this scattering geometry are also given in Table II.

Figure 3 shows spectra obtained in the geometry just described in the second half of Table II for CaF_2. The incident polarization is [001] and no

Table II. Expected Brillouin intensities for two scattering geometries probing phonons propagating along [110]. (i) $\vec{k}_i = -\vec{k}_s$//[110] and (ii) k_i//[100], k_s//[010].

(i)

	e_i = [001] e_s = [001]	e_i = [001] e_s = $1/\sqrt{2}[1\bar{1}0]$	e_i = $1/\sqrt{2}[1\bar{1}0]$ e_s = [001]	e_i = $1/\sqrt{2}[1\bar{1}0]$ e_s = $1/\sqrt{2}[1\bar{1}0]$
long	$(2p_{12})^2$	0	0	$(p_{11}+p_{12}-2p_{44})^2$
Transv (1)	0	0	0	0
Transv (2)	0	0	0	0

(ii)

	e_i = [010] e_s = [100]	e_i = [010] e_s = [001]	e_i = [001] e_s = [100]	e_i = [001] e_s = [001]
long	$(2p_{44})^2$	0	0	$(2p_{12})^2$
Transv 1	0	$2(p_{44})^2$	$2(p_{44})^2$	0
Transv 2	0	0	0	0

analyzer was used so that e_s is either [100] or [001]. A comparison of Figs. 3a-c shows the importance that multipassing has on the contrast of the instrument (note the logarithmic intensity scale.) The advantage of the tandem arrangement is shown in Figs. 3d-f; in this case it just simplifies the assignment of the Brillouin peaks, however in cases where many peaks are present, the elimination of half of them becomes a very desirable feature. The disadvantage, i.e., loss of intensity, on going to the tandem is also evident.

From the frequency shifts determined in Fig. 3, the wavevector given in Fig. 2a and using Eq. 4 we calculate the velocity v. The effective elastic constants X are calculated using Eq. 5. Since from Table II we know that we expect to observe only the longitudinal and the transverse 1 modes, the values of X can be assigned to $(C_{11} + C_{12} + 2C_{44})/2$ and C_{44} (see Table I).

IV. BRILLOUIN SCATTERING FROM DIAMOND ANVIL CELLS

Figure 4 is a schematic view of the diamonds, gasket and diamond supports of a diamond anvil cell. From such a cell it is possible to use any one of the openings for the incident laser beam and also collect the scattered beams through any of them. There are however only two particular geometries that are commonly used; one is backscattering as indicated in

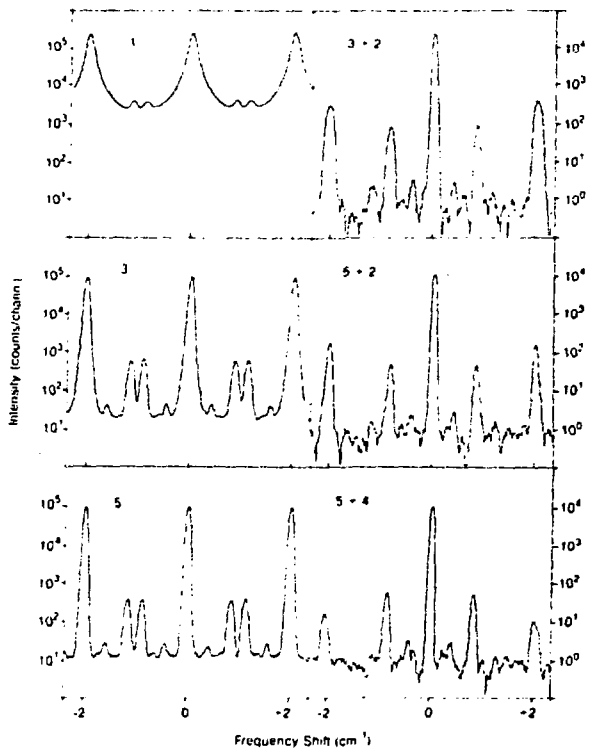

Fig. 3. Spectra recorded with different configurations of the Fabry-Perot from a sample of CaF_2 with k_i//[100], k_s//[010] and e_i//[001]. The spectra on the left are for 1, 3, and 5 passes on a single instrument, those on the right are in tandem operation the two numbers indicating the number of passes on each instrument.

Fig. 2b and shown by the double arrow in figure 4; the other, indicated by the single arrows, corresponds to the geometry of Fig. 2c and will be referred to as the platelet geometry. The latter of these two geometries has a number of features which make it more attractive than backscattering: there is less parasitic light scattered into the detector so that a Fabry-Perot of lower contrast is required, information is obtained on transverse as well as longitudinal modes (as shown in Table II, in backscattering one seldom couples to transverse modes), and the refractive index is not needed (see Fig. 2c) for data analysis. The only advantage of backscattering is that cells that do not have all the openings shown in Fig. 4 but only those along the cell axis, usually are capable of reaching higher pressures. Table III lists the experiments which have been reported to date[10-31] and indicates the material studied, the scattering geometry, and the maximum pressure achieved. As can be seen from the table, experiments performed in the backscattering geometry have, on the average, achieved higher pressures.

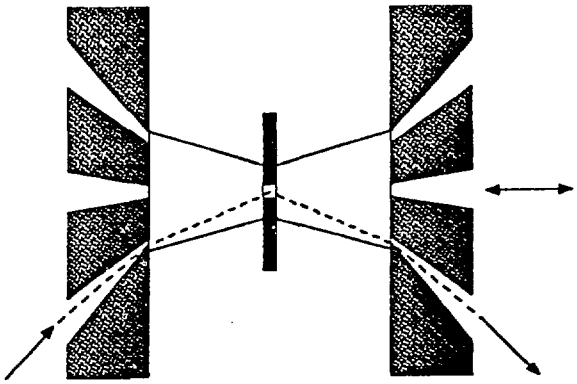

Fig. 4. Schematic diagram of the heart of a diamond anvil cell showing the diamond seats, the diamonds and the gasket. The arrows indicate possible scattering geometries.

Table III. Systems studied to date at high pressures using Brillouin scattering.

Material	Scattering Geometry	Max Pressure (GPa)	Ref.
NaCl	platelet	4	10
H_2, D_2	platelet	20	11
a-SiO_2	platelet	13	12
GaS	back.	18	13,14
Mg_2SiO_4	platelet	4	15
H_2O, D_2O	back.	74	16,17,18
a-SiO_2	back.	17	19,20
TiO_2	back.	14	21
N_2	back.	20	22
Ar	back.	35	23,24
HF	platelet	12	25
He	back.	20	26
CH_4	back.	32	27
CS_2	platelet	7	28
NH_3	back.	20	29
Kr	back.	33	30
a-GeO_2	back.	20	31
a-B_2O_3	back.	15	31
a-As_2S_3	back.	5	31
Lucite	back.	14	31

Once spectra have been recorded the measured frequency shifts can be converted into sound velocities using Eq. 4 and the appropriate wavevector from Fig. 2. For backscattering, the calculation of the wavevector requires a knowledge of the refractive index versus pressure which is not known for most materials.[32] For most materials however this problem is not as serious as might appear at first sight; the refractive index is a weak function of the density, and for many substances the density is known as a function of pressure so that a reliable estimate of the refractive index (e.g., using the Clausius-Mossotti equation) can be made. Estimates for specific substances can be found in Refs. 16, 24, and 26.

Once the velocities have been determined, the effective elastic constant is obtained using Eq. 5. In order to associate the measured effective elastic constant with a specific combination of C_{ij}'s it is necessary to know the crystal orientation within the DAC. For samples that are placed in the cell in solid form this can be easily done,[13-15,21] for samples that solidify in the cell under pressure, there is no control over the crystal orientation and hence data analysis is not straightforward. Specific cases will be discussed in the next section.

V. EXPERIMENTAL RESULTS FOR H_2, N_2, Ar AND He

H_2 and D_2

Brillouin scattering results from H_2 and D_2 up to pressures of 20 GPa have been reported by Shimizu et al., in Ref. 11. Figure 5 shows the

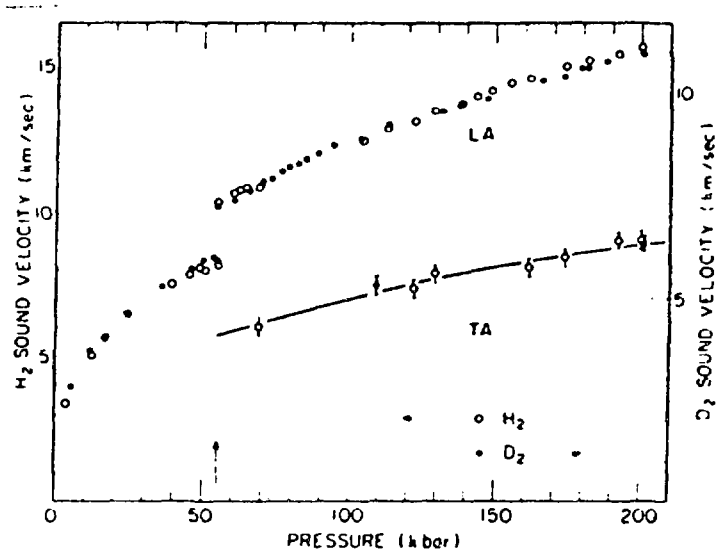

Fig. 5. (From Ref. 11.). Sound velocity of n-H_2 and n-D_2 with pressure. Open circles, n-H_2; solid circles, n-D_2. The vertical scale for n-H_2 sound velocity is $\sqrt{2}$ times that for the n-D_2 sound velocity. LA, longitudinal acoustic mode; TA, transverse acoustic mode. Vertical arrow indicates the fluid--solid phase transition point (55 kbar).

results for the sound velocities obtained from their results (because they used the 'platelet' geometry, their results are not dependent on an estimate of the refractive index). In this case the usual next step of determining the elastic constants using Eq. 5, is not possible because the density is not known. However it is possible to use the Brillouin results to obtain the density by recalling that the bulk modulus (B) is related to the density (ρ) through

$$B_T = \rho \left.\frac{dP}{d\rho}\right|_T = B_S/\gamma \tag{9}$$

where P is the pressure, subscripts T and S indicate isothermal and adiabatic respectively and γ is the ratio of specific heats. In the liquid B_S is equal to the product of the density times the square of the measured sound velocity so it is straight forward to integrate Eq. 9 to yield

$$\rho_{P_1} = \rho_{P_0} + \int_{P_0}^{P_1} (\gamma/v^2)\, dP \tag{10}$$

The most serious problem with integrating this equation is the choice of γ which has not been measured. With a reasonable choice of γ(= 1.07) the density of fluid H_2 was obtained in Ref. 11. The use of Eq. 9 for the solid is not as straight forward since B_S is no longer simply related to a specific measured velocity. For a cubic crystal

$$B = \frac{1}{3}(C_{11} + 2C_{12}) \tag{11}$$

for an isotropic solid this can also be written

$$B = C_{11} - \frac{4}{3} C_{44} \tag{12}$$

Since for an isotropic solid $C_{11} = \rho v_L^2$ and $C_{44} = \rho v_T^2$, where subscripts L and T indicate longitudinal and transverse respectively, if the solid were isotropic Eq. 9 could indeed be integrated. The room temperature structure of solid H_2 at these high pressures has not been experimentally determined, however, independent of this fact, the Brillouin results indicate that the solid is close to being elastically isotropic. This fact can be ascertained by the fact that the experimental results have little spread; if the solid were anisotropic, then since in each run a different crystallographic direction would be probed, a slightly different velocity would be measured. Another problem with using Eq. 9 to obtain the density of the solid is that the initial density (i.e. just after freezing) is not known either, the only simplifying feature in the solid is that it is a good approximation to take $\gamma = 1$. By making an estimate of the density change on freezing, and assuming elastic isotropy, the authors were able to calculate the density of H_2 up to 20 GPa. The density results are still awaiting confirmation by more direct techniques such as x-rays.

Up to this point then, Brillouin scattering has yielded the only reliable information on the equation of state of high density H_2.

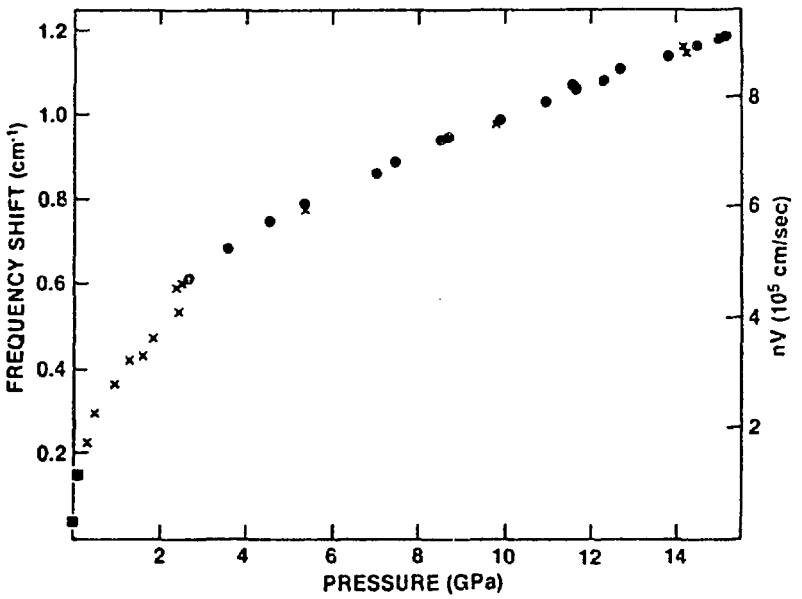

Fig. 6. Brillouin frequency shift from nitorgen vs. pressure in the range 0-15 GPa. Dots and crosses are for increasing and decreasing pressures, respectively. Squares are calculated from data in the literature.

$\underline{N_2}$

Another way in which Brillouin scattering can contribute to our understanding of a material under pressure is exemplified by the results on N_2 reported in Ref. 22. Figure 6 shows the Brillouin frequency shift and the calculated product of the sound velocity times the refractive index. As for the case of H_2, the freezing transition at ~2.5 GPa is clearly observable. Above 2.5 GPa in the solid only the longitudinal mode is seen because the experiments were performed in the backscattering geometry. Figure 7 shows the Brillouin results at higher pressures where a discontinuity in the frequency is observed. This jump in frequency is interpreted as a phase change since there is no other reason that could explain it. The existence of a phase change is further confirmed by the fact that at the same pressure at which the frequency change occurs, there are certain visible changes that are observed concomitantly.

A surprising fact about the above mentioned phase change is that it is not observed in Raman scattering experiments.[33-35] These experiments [33-34] indicate a phase transformation at ~5.4 GPa, which is not observed in the Brillouin experiment; at ~20 GPa a further gradual splitting is observed in the Raman lines[35] but because of its gradual nature it is not clear if it is a phase change or simply due to non-hydrostatic pressure. A complete understanding of the experimental results is still awaiting further investigation.

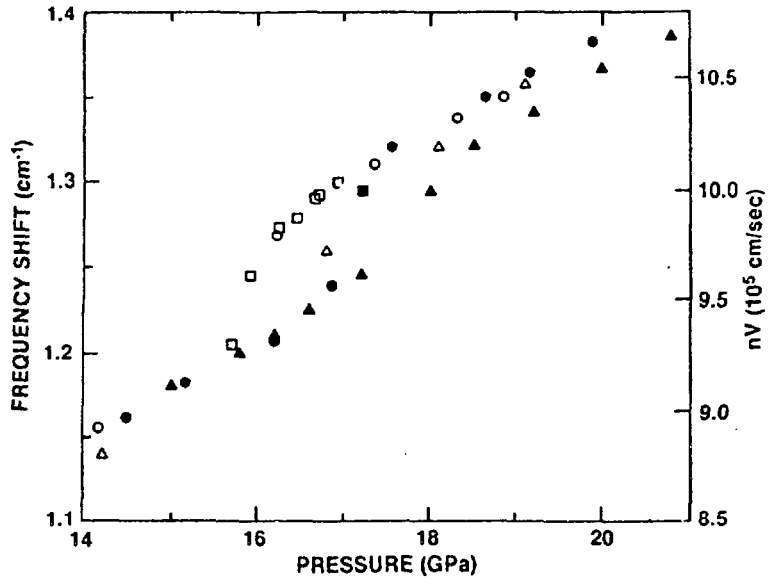

Fig. 7. Brillouin frequency shift from nitorgen vs. pressure in the range 14-21 GPa. Full and open symbols are for increasing and decreasing pressures respectively. Different symbols correspond to different runs.

Argon

It is interesting to note that even for the relatively simple systems referred to above, viz. H_2 and N_2, there are no theoretical calculations with which to compare the Brillouin scattering results. This fact is a clear statement of the level of our current understanding of systems at high pressures, and indicates that in order for a comparison to be made between theory and experiment, it is necessary to study even simpler systems. From this point of view Ar is perhaps one of the most ideally suited; because of its closed electronic shell it is well described by a spherically symmetric potential and it is heavy enough so that quantum effects can be neglected. From the experimental standpoint however it is not as well suited; because it crystallizes in the fcc structure it has no Raman or IR active modes thus excluding two of the most powerful techniques used in high pressure research. The only (but perhaps the most important) measured property of Ar at high pressures is the density derived from x-ray studies.[36-38]

The Brillouin scattering results, obtained in the backscattering[23,24] geometry and shown in Fig. 8, clearly show the fluid to solid phase transition at ~1.4 GPa. Above this pressure the spread in the experimental points reflects the elastic anisotropy of fcc Ar and the fact that in different runs we probe different crystallographic directions. In the liquid our results agree with those obtained with ultrasonic techniques.[39] In order to transform the frequency shifts to velocities, an estimate of the refractive index was made; this estimate has since been found to agree with

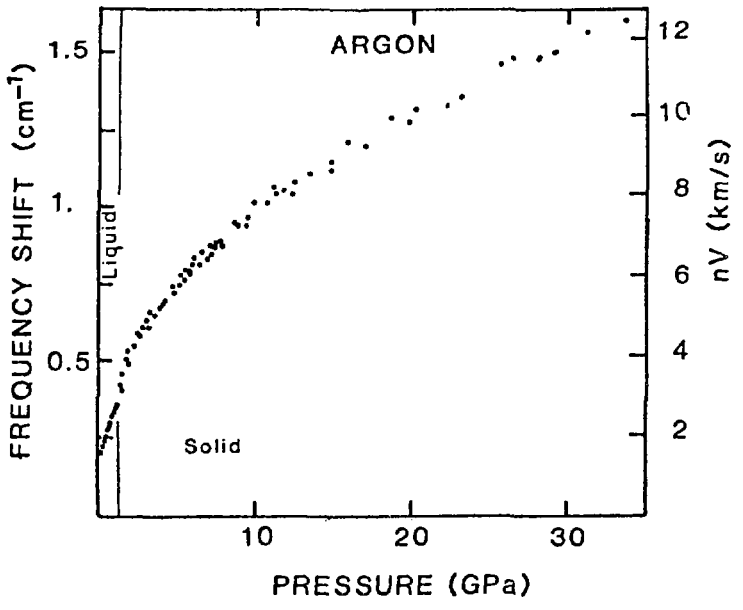

Fig. 8. Brillouin frequency shift from argon as a function of pressure (left hand scale) and the corresponding values of the product of the refractive index times the sound velocity (right hand scale).

experimental measurements up to 15 GPa.[32] As explained before, from the measured frequency shifts, the refractive index and the measured density[36-38] the effective elastic constants can be obtained and are shown in Fig. 9. In spite of the fact that the orientation of the crystallites in the cell are not known, the results shown in Fig. 9 can be used to obtain information on specific elastic constants by assuming that in the large number of experiments performed, all directions will be randomly probed. With this assumption and the fact that in argon it is known that the largest longitudinal elastic constant is along a [111] direction, and the smallest one is along a [100], the envelope curves shown in Fig. 9 can be taken to be equal to $C^* = (C_{11} + 2C_{12} + 4C_{44})/3$ and C_{11}, respectively. Combining this information with the bulk modulus (Eq. 11) derived from the density measurements [36-38] using Eq. 9, the three independent elastic moduli can be obtained and are shown in Table IV.

A detailed comparison of theoretical calculations with both the Brillouin and density results was presented in Ref 24. It was reported that even though two-body potentials could be found that would reproduce the measured density and other potentials that would produce good agreement with the elastic properties, no potential was found that would yield satisfactory results for both properties. The question as to whether a potential was not found simply due to insufficient searching or whether it is not possible on physical grounds, can also be answered by a more detailed analysis of the Brillouin results. It can be shown that for any crystal in which the atoms are located at sites with inversion symmetry and in which only central

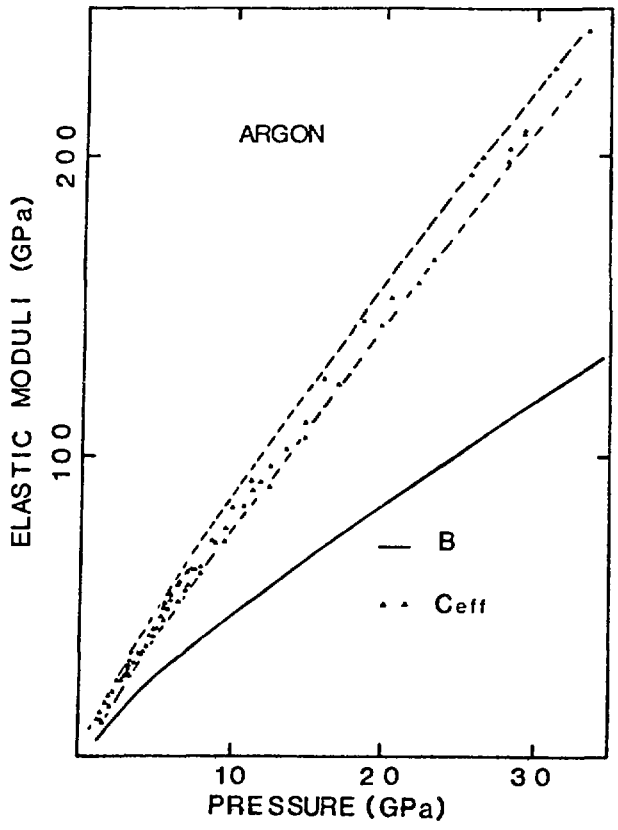

Fig. 9. Elastic moduli of solid argon vs. pressure. Triangles: effective longitudinal moduli (defined in text) measured by Brillouin scattering; the two dashed lines represent the envelope curves we used to determine C_{11} and C^* (see text). Solid line: bulk modulus determined by x-ray measurements (Refs. 36-38).

Table IV. Elastic constants of solid argon versus pressure all quantities in GPa, and $\delta = (C_{44} - C_{12} + 2P)/C_{12}$.

P	C_{11}	C_{44}	C_{12}	δ
2	16 ± 1	7.5 ± 1.5	8.4 ± 2.0	0.41 ± 0.4
4	32 ± 1	11.6 ± 1.1	16.3 ± 1.3	0.20 ± 0.15
6	48 ± 1	17.6 ± 1.1	21.9 ± 1.3	0.35 ± 0.11
10	74 ± 1	27.1 ± 1.1	33.3 ± 1.3	0.41 ± 0.07
15	109 ± 2	41 ± 2	44 ± 2	0.61 ± 0.09
20	142 ± 2	54 ± 2	54 ± 2	0.74 ± 0.07
25	178 ± 2	68 ± 2	63 ± 3	0.87 ± 0.08
30	211 ± 2	80 ± 2	71 ± 3	0.97 ± 0.07

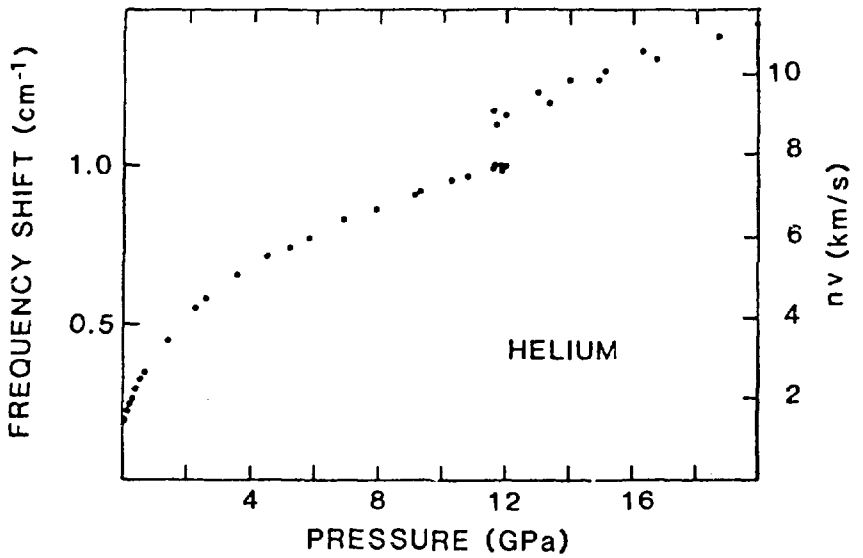

Fig. 10. Brillouin frequency shift from He vs. pressure. The product of the sound velocity times the refractive index is given on the right hand side.

forces are important, the Cauchy relationship must hold, viz.

$$C_{44} - C_{12} + 2P = 0 \ . \qquad (13)$$

Since fcc Ar certainly satisfies the first requirement, if Eq. 13 does not hold it implies that non central forces play a significant role and consequently that any accurate description of the elastic properties must involve forces that can not be described in terms of "spherically symmetric" interaction potentials. Table IV gives values for δ which is a measure of the deviations from Eq. 13, these values show that at high pressures there are large deviations and consequently that any future calculations of dense argon must contain either non-central forces or many body forces and that there is no point in trying to refine an effective two body potential.

Helium

Of the systems which are of interest in high pressure studies He is perhaps the one about which least is known. At room temperature it has no Raman or IR active modes and its cross section for x-rays is so small that it has not yet been possible to determine its density by this technique. Above 2 GPa the only property that has been experimentally determined is the melting curve[40,41]. Because of this lack of information on He the recently reported Brillouin scattering results[26] have provided very useful information. Figure 10 shows the Brillouin frequency shift from He up to 20 GPa.

As for the other materials described here, the transition from fluid to solid at 12 GPa is clearly observable and the spread in the points in the solid give an indication of the elastic anisotropy. In this case however, because of the few runs reported, one cannot assume that all crystallographic directions have been probed. The measured velocity of sound in the fluid can be compared with the sound velocity derived from the calculated equation of state. The density as a function of pressure has been calculated[32,43] using two different potentials to describe the He-He interaction but both calculations yield velocities considerably higher than the experimental one. It was concluded from this that the calculated equations of state could not be correct and therefore, using the same procedure as described earlier for H_2, the density of the fluid was calculated from the Brillouin results. The density as a function of pressure is shown in Fig. 11 showing the discrepancy between the density calculated using the Brillouin results and that calculated with two-body potentials. More recent calculations[44] which include three body interactions produce much better agreement with experiment.

Work supported by the U.S. Department of Energy, BES-Materials Sciences, under Contract ØW-31-109-ENG-38.

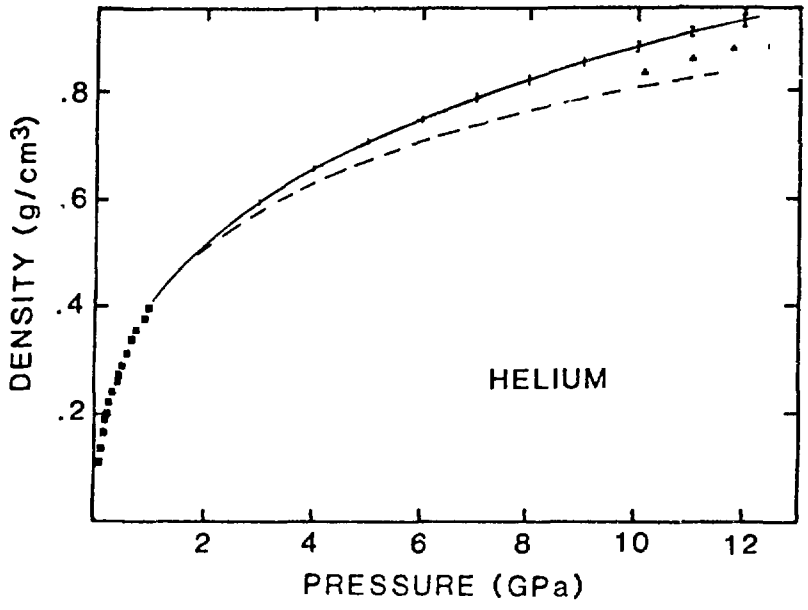

Fig. 11. Density vs. pressure for fluid He at room temperature. The full line is the Brillouin result, the dashed line, triangles and circle are calculations and the squares are experimental values.

REFERENCES

1. M. Born and K. Huang, in "Dynamical Theory of Crystal Lattices", Oxford Univ. Press, London (1968).

2. W. Hayes and R. Loudon, in "Scattering of Light by Crystals", New York, NY (1978).
3. H. Z. Cummins and P. E. Schoen in "Laser Handbook", ed. by T. Arecchi and E. O. Schulz-Dubois, North-Holland, Amsterdam (1972), p. 1029.
4. L. Brillouin, Compt. Rend. CLVIII, 1331 (1914); Ann. Phys. (Paris) 17:88 (1921).
5. E. Gross, Nature 126:201 (1930).
6. C. V. Raman, Indian J. Phys. 2:387 (1928).
7. J. R. Sandercock in "Light Scattering in Solids", ed. M. Balkanski Flammarion, Paris, (1971), p. 9.
8. J. R. Sandercock in "Topics in Applied Physics Vol. 51: Light Scattering in Solids III," ed. M. Cardona and G. Güntherodt, Springer, NY (1982).
9. See for example C. Kittel "Introduction to Solid State Physics" Wiley, NY, (1971).
10. C. H. Whitfield, E. M. Brody, and W. A. Bassett, Rev. Sci. Instrum. 47:942 (1976).
11. H. Shimizu, E. M. Brody, H. K. Mao, and P. M. Bell, Phys. Rev. Lett. 47:128 (1981).
12. J. Schroeder, K. J. Dunn, and F. P. Bundy in Proc. of the Eight AIRAPT Conference on High Pressure in Research and Industry, Uppsala, 1981, ed. by C. M. Backman, T. Johannisson, and L. Tegner, p. 259.
13. A. Polian, J. M. Besson, M. Grimsditch, and H. Vogt, Appl. Phys. Lett. 38:334 (1981).
14. A. Polian, J. M. Besson, M. Grimsditch, and H. Vogt, Phys. Rev. B25:2767 (1982).
15. H. Shimizu, W. A. Bassett, and E. M. Brody, J. Appl. Phys. 53.620 (1982).
16. A. Polian and M. Grimsditch, Phys. Rev. B27:6409 (1983).
17. A. Polian and M. Grimsditch, Phys. Rev. Lett. 52:1312 (1984).
18. A. Polian and M. Grimsditch, Phys. Rev. B29:6362 (1984).
19. M. Grimsditch, Phys. Rev. Lett. 52:2379 (1984).
20. M. Grimsditch, Phys. Rev. B34:4372 (1986).
21. A. Polian and M. Grimsditch, J. de Physique Lett. 45:L1131 (1984).
22. M. Grimsditch, Phys. Rev. B32:514 (1985).
23. A. Polian and M. Grimsditch, Physica 139&140B:187 (1986).
24. A. Polian, P. Loubeyre, and M. Grimsditch, Phys. Rev. B33:7192 (1986).
25. S. A. Lee, D. A. Pinnick, S. M. Lindsay, and R. Hanson, Phys. Rev. B34:2799 (1986).
26. A. Polian and M. Grimsditch, Europhysics Lett. 2:849 (1986).
27. P. Hebert, A. Polian, P. Loubeyre, and R. Letoullec, Phys. Rev. B (Accepted).
28. H. Shimizu, S. Sasaki, and T. Ishidate, J. Chem. Phys. 86:7189 (1987).
29. M. Gauthier, Ph. Pruzan, J. C. Chervin, and A. Polian, Sol. State Commun. (to be published)
30. A. Polian, J. M. Besson, M. Grimsditch, and W. A. Grosshans, (to be published).
31. M. Grimsditch, R. Bhadra, and Y. Meng, (to be published).
32. M. Grimsditch, R. Letoullec, A. Polian, and M. Gauthier, J. Appl. Phys. 60:3479 (1986).
33. R. LeSar, S. A. Ekberg, L. H. Jones, R. L. Mills, L. A. Schwalbe, and D. Schiferl, Solid State Commun. 32:131 (1979).

34. L. A. Schwalbe, D. Schiferl, R. L. Mills, L. H. Jones, S. Ekberg, D. T. Cromer, R. LeSar, and J. Shaner in High Pressure in Science and Technology, ed. by B. Vodar and P. Marteau (Pergamon, NY, 1980), Vol. 2, p. 612.
35. S. Buchsbaum, R. Mills, and D. Schiferl, J. Phys. Chem. 88:2522 (1984).
36. R. M. Hazen, H. K. Mao, L. W. Finger, and P. M. Bell, Carnegie Inst. Washington Yearb. 79:348 (1980).
37. G. Zou, H. K. Mao, and P. M. Bell, Carnegie Inst. Washington Yearb. 81:392 (1982).
38. J. Xu, H. K. Mao, and P. M. Bell, High Temp. High Pressures 16:495 (1984).
39. D. H. Liebenberg, R. L. Mills, and J. C. Bronson, J. Appl. Phys. 45:741 (1974).
40. J. M. Besson and J. P. Pinceaux, Science 206:1073 (1979).
41. P. Loubeyre, J. M. Besson, J. P. Pinceaux, and J. P. Hansen, Phys. Rev. Lett. 49:1172 (1982).
42. J. P. Hansen, Phys. Rev. A2:221 (1970).
43. R. Aziz, V. P. S. Nain, J. S. Carley, W. L. Taylor, and G. T. McConville, J. Chem. Phys. 70:4330 (1979).
44. P. Loubeyre (to be published).